Available online at www.sciencedirect.com

SciVerse ScienceDirect

Ceramics International 39 (2013) 7677–7683

CERAMICS INTERNATIONAL

www.elsevier.com/locate/ceramint

The optical properties of hydrophilic Hf-doped HfO_2 nanoceramic films

Su-Shia Lin*, Han-Ru Li

Department of Applied Materials and Optoelectronic Engineering, National Chi Nan University, Puli, Nantou Hsien 54561, Taiwan, ROC

Received 15 November 2012; received in revised form 2 February 2013; accepted 6 March 2013
Available online 21 March 2013

Abstract

The Hf-doped HfO_2 (HfO_2:Hf) nanoceramic films were deposited by simultaneous rf magnetron sputtering of HfO_2 and dc magnetron sputtering of Hf. By doping with Hf, the lowest oxidation state of Hf (Hf^{0+}) presented preferentially and changed the hydrophobicity of HfO_2 film into hydrophilicity. On comparing with the HfO_2 film, the optical transmission of HfO_2:Hf film was higher and strongly increased with pressure, especially in the ultraviolet region and near infrared region. At higher pressure, HfO_2:Hf film exhibited better hydrophilicity, higher linear refractive index and lower stress-optical coefficient.

Keywords: Film; Sputtering; Hydrophilicity; Transmission

1. Introduction

Hafnium (Hf) belongs to Group 4 elements, hence HfO_2 and its composite films have been investigated for various optical and electrical applications [1]. The HfO_2 thin films exhibit hydrophobicity and also have many useful practical applications ranging from self-cleaning activity of window sheets to anticlouding effects in bathrooms mirrors, car windows and fender mirrors [2]. HfO_2 thin films have been prepared by different techniques, including sol–gel [3,4], electron beam evaporation [5], ion beam assisted deposition [6], chemical vapor deposition [7], sputtering [8,9] and atomic layer deposition (ALD) [10].

Among these techniques, magnetron sputtering provides more advantages in controlling the microstructure and composition of the films [11]. The characteristics of films are affected by the preparation conditions such as working pressure, substrate temperature, types of substrates, and the thickness of the films [12]. Doping metal ions has been largely employed for enhancing the properties of HfO_2 [13–15]. In this study, Hf-doped HfO_2 (HfO_2:Hf) nanoceramic films were prepared by simultaneous rf magnetron sputtering of HfO_2 and dc magnetron sputtering of Hf. The influence of working pressure on the HfO_2:Hf films with respect to the hydrophilicity and optical properties was investigated.

2. Experimental procedures

The HfO_2:Hf nanoceramic films were deposited on glass (Eagle 2000) by simultaneous rf magnetron sputtering of HfO_2 and dc magnetron sputtering of Hf. The dimension of the glass substrates was 24 mm × 24 mm × 1.1 mm. Before deposition, the substrates were ultrasonically cleaned in alcohol, rinsed in deionized water and dried in nitrogen. Two circular targets were used (5 cm diameter, 5 mm thickness); the first was sintered stoichiometric HfO_2 (99.95% purity), and the other was metallic Hf (99.95% purity).

The sputtering was performed in Ar atmosphere with a target-to-substrate distance of 15 cm. A turbo-molecular pump, backed by a rotary pump, was used to achieve a base pressure of 1.3×10^{-4} Pa. For the deposition of the films, the substrates were not heated. The working pressure was 1–3 Pa. An rf power (13.56 MHz, RGN-1302, ULVAC, Japan) of 120 W was supplied to the HfO_2 target, and a dc power (DCS0052B, ULVAC, Japan) of 0–8 W was applied to the Hf target. No external bias voltage was applied to the substrate. The rotating speed of the substrate was 20 rpm, and the thickness of films was maintained at 100 nm.

Film thickness was measured using a surface profiler (Alpha-Step 500, TENCOR, Santa Clara, CA). X-ray

*Corresponding author. Tel.: +886 49 2910 960x4771; fax: +886 49 291 2238.
E-mail address: sushia@ncnu.edu.tw (S.-S. Lin).

0272-8842/$ - see front matter © 2013 Elsevier Ltd and Techna Group S.r.l. All rights reserved.
http://dx.doi.org/10.1016/j.ceramint.2013.03.020

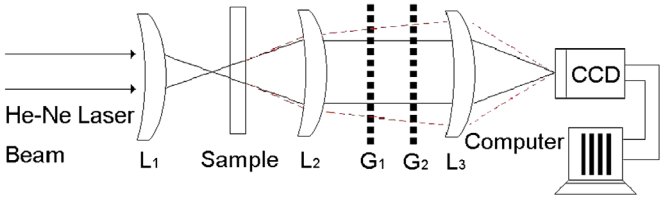

Fig. 1. The experimental set-up for measuring nonlinear refractive index by the Moiré deflectometry technique.

diffraction (XRD; Rigaku D/MAX2500, Japan) was used to study the crystal structure. Elemental compositions were investigated by X-ray photoemission spectroscopy (XPS; PHI 5000 VersaProbe, Japan). The optical transmission spectra of films in the ultraviolet–visible–near infrared (UV–VIS–NIR) region were obtained using a spectrophotometer (HP 8452A diode array spectrophotometer, Hewlett Packard, Palo Alto, CA). The water contact angles on samples were measured by a contact angle meter (Model 100SB, Sindatek, Taiwan). Surface morphologies and surface roughness were examined by atomic force microscopy (NS3a controller with D3100 stage, Digital instruments, Santa Barbara, CA). Linear refractive indices of samples were recorded using a spectrometer (MP100-ST, Fremont, CA). Stress was measured by the Nano Indenter XP System (MTS Systems Corporation, MN, USA).

Moiré deflectometry is a powerful tool for measuring the nonlinear refractive indices of materials. The main advantages of the Moiré deflectometry technique are its extreme experimental simplicity, lower cost and lower sensitivity to external disturbances than other interferometric methods. In this study, this method was applied to measure the nonlinear refractive indices of HfO_2:Hf films on glass substrates under illumination with a 5-mW He–Ne laser (λ=632.8 nm).

Fig. 1 shows the Moiré deflectometry experimental set-up that is used to measure the nonlinear refractive indices of HfO_2:Hf films on glass substrates. Lens L_1 focused a 5-mW He–Ne laser beam (wavelength of 632.8 nm), which was re-collimated by lens L_2. The focal lengths of lenses L_1, L_2 and L_3 were all −250 mm. Two similar Ranchi gratings, G_1 and G_2 with a pitch of 0.1 mm were used to construct the Moiré fringe patterns. The distance between the planes of G_1 and G_2 was set to 64 mm, which is one of the Talbot distances of the used gratings. The Talbot distances satisfy $z_t = tp^2/\lambda$ where p is the periodicity of the grating; λ is the wavelength of light, and t is an integer. In this work, the Moiré fringes were clearly formed at a Talbot distance of $z_{t=4} \approx 64$ mm. The Moiré fringe patterns were projected onto a computerized CCD camera by lens L_3, which was placed at the back of the second grating.

3. Results and discussion

Fig. 2 shows the X-ray diffraction patterns of HfO_2 and HfO_2:Hf films deposited at a pressure of 1.5 Pa. XRD analysis was conducted on the films using a Rigaku D/MAX2500 goniometer with 18 kW rotating anode X-ray, equipped with a thin film attachment unit. The equipment was operated with Cu

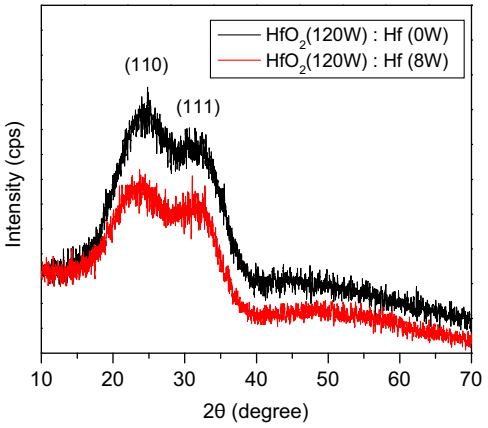

Fig. 2. The X-ray diffraction patterns of HfO_2 and HfO_2:Hf films deposited at a pressure of 1.5 Pa.

Kα (λ = 1.5418 Å) radiation at 40 kV, 100 mA and a scanning speed of 4° min^{-1} at an incident angle of 3°. The interval of the scan was 0.01° and the scanning range was 10°–70°. In Fig. 2, it could be found that there were two broad diffraction peaks (110) and (111) corresponding to the nanocrystalline monoclinic HfO_2 film. On comparing with the HfO_2 film, the HfO_2:Hf film showed poor nanocrystallinity. Furthermore, the locations of the measured diffraction peaks shifted toward the lower diffraction angle by doping with Hf.

Lohmann et al. [16] studied TiB_2 coatings on steel and reported that compressive stress of the lattice in a direction parallel to the surface could affect the lattice perpendicular to the surface. Similarly, the crystallite was distorted by excess Hf atoms as interstitial atoms in the lattice of HfO_2:Hf film. Also, the HfO_2:Hf film suffered the compressive stress of the lattice in a direction parallel to the surface. Thus, it could result in the increase in interplanar spacing. By following Bragg's law [17]:

$$\lambda = 2d \sin\theta \quad (1)$$

where d is the interplanar spacing and θ is the diffraction angle. It could be understood that the increase in interplanar spacing resulted in decreasing diffraction angle. Therefore, the (110) and (111) peaks shifted toward the lower diffraction angle by doping with Hf, an indication that the structure of HfO_2:Hf film became more random.

Table 1 shows the elemental composition of HfO_2:Hf films under different sputtering conditions analyzed by XPS. The Hf content of the deposited films increased with dc power. The O/Hf atomic ratio decreased with dc power. However, there is no difference in the elemental composition of HfO_2:Hf films deposited at various pressures. This suggested that the deposited films became far from stoichiometric by increasing dc power.

The bonding conditions of oxygen on the surfaces of HfO_2 film and HfO_2:Hf film were investigated by XPS spectra. Fig. 3 shows O 1s photoelectron peaks in the XPS spectra of (a) HfO_2 and (b) HfO_2:Hf films deposited at a pressure of 1.5 Pa. In Fig. 3a, the O 1s peak was composed of two peaks

Table 1
Elemental composition of HfO_2:Hf films under different sputtering conditions analyzed by XPS.

rf power (W)	dc power (W)	Pressure (Pa)	O content (at%)	Hf content (at%)	O/Hf
120	0	1.5	66.1	33.9	1.95
120	8	1.0	64.4	35.6	1.81
120	8	1.5	64.4	35.6	1.81
120	8	2.0	64.4	35.6	1.81
120	8	2.5	64.4	35.6	1.81
120	8	3.0	64.4	35.6	1.81

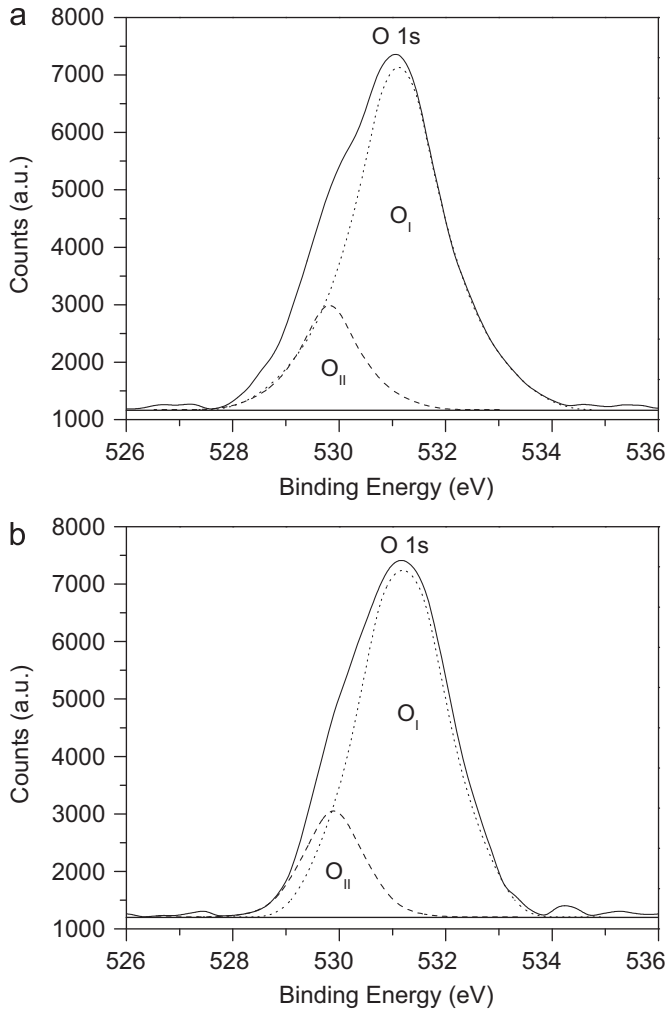

Fig. 3. O 1s photoelectron peaks in the XPS spectra of (a) HfO_2 and (b) HfO_2:Hf films deposited at a pressure of 1.5 Pa.

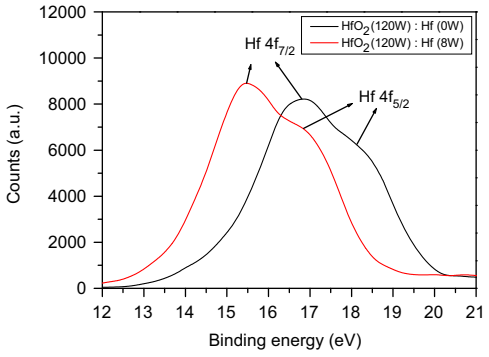

Fig. 4. Hf 4f photoelectron peaks in the XPS spectra of HfO_2 and HfO_2:Hf films deposited at a pressure of 1.5 Pa.

(O_I and O_{II}). The peak (O_I) at 531.1 ± 0.01 eV maybe due to oxygen in HfO_2 [18,19]. The peak (O_{II}) at 529.8 ± 0.02 eV was probably due to oxygen in HfO. In Fig. 3b, the O 1s peak was composed of two peaks (O_I and O_{II}). The peak (O_I) at 531.1 ± 0.08 eV maybe due to oxygen in HfO_2, and the peak (O_{II}) at 529.8 ± 0.07 eV was probably due to oxygen in HfO.

We defined the relative strength of a peak as the ratio of its area to the total area of O_I and O_{II} peaks. According to Fig. 3a and b, the relative strength of O_I was relatively high and similar. It suggested that Hf atoms in HfO_2 crystalline were not substituted favorably by doping with Hf. It also indicated that excess Hf atoms were as interstitial atoms in the lattice of HfO_2:Hf film.

The bonding conditions of hafnium on the surfaces of HfO_2 film and HfO_2:Hf film were investigated by XPS spectra. Fig. 4 shows Hf 4f photoelectron peaks in the XPS spectra of HfO_2 and HfO_2:Hf films deposited at a pressure of 1.5 Pa. Hf $4f_{7/2}$ of the Hf^{0+} is at ~14.0 eV in the binding energy scale [20]. Hf $4f_{7/2}$ at ~16.2 eV has been suggested as the Hf $4f_{7/2}$ of the Hf^{2+} from HfO [21]. Hf $4f_{7/2}$ at ~17.6 eV has been suggested as the Hf $4f_{7/2}$ of the Hf^{4+} from HfO_2 [22]. In Fig. 4, the major peak at 16.8 eV and the shoulder peak at 18.2 eV corresponded to Hf $4f_{7/2}$ and Hf $4f_{5/2}$, which indicated that the hafnium in the HfO_2 film may form mixed valence of Hf^{2+} and Hf^{4+}. The binding energy of Hf $4f_{7/2}$ decreased from 16.8 to 15.4 eV when dc power increased from 0 to 8 W. The origins of the binding energy shift are suggested by a number of factors, such as the charge transfer effect, presence of electric fields, environmental charge density, and hybridization [23]. Among these, charge transfer is regarded as the dominant mechanism to cause binding energy shift [23]. According to the charge transfer mechanism, removing an electron from the valence orbital generates an increase in the core electron's potential and finally leads to a chemical binding energy shift [23].

The peaks shifted to lower bonding energy after doping Hf, which indicated that metallic hafnium (Hf^{0+}) presented preferentially and as interstitial atoms in the lattice of HfO_2:Hf film. The results suggested that the deposited film was far

from stoichiometric by doping with Hf. This was in agreement with the results of Table 1.

Fig. 5 shows the transmission in the UV–VIS–NIR region of HfO_2 and HfO_2:Hf films deposited at a pressure of 1.5 Pa. The transmission in the visible region all exceeded 80%. The transmission increased obviously at longer wavelength by doping with Hf. The difference in transmission between the films was related to the difference in the porosity [24]. For HfO_2:Hf film, metallic hafnium (Hf^{0+}) presented preferentially, as interstitial atoms in the lattice of film, and corresponded to higher transmission. The light-absorbing defects were removed by interstitial atoms. Therefore, the increase in transmission was probably due to the reduced porosity [25].

The water contact angle on HfO_2 film was 90.6°, which exhibited hydrophobicity. After doping Hf, the water contact angle decreased to 73.5°, and exhibited hydrophilicity. Hf^{2+} was more favorable to form in the hydrophobic HfO_2 film [2]. By doping with Hf, Hf^{0+} presented preferentially in the film and exhibited hydrophilicity. The bonding condition of hafnium on the surface of HfO_2 film was the dominant factor in this study. Therefore, a control of lowest oxidation state of Hf (Hf^{0+}) is a way to change the hydrophobicity of HfO_2 film into hydrophilicity.

Fig. 6 shows water contact angles on HfO_2:Hf films deposited at various pressures. Wettability of a solid surface with liquids is not only governed by its chemical properties but also by its geometry. Hydrophilicity is well known to be enhanced by fine roughness [26,27]. Therefore, a control of surface microstructure of the films is a way to improve the hydrophilicity. The water contact angle decreased with pressure. It suggested that the hydrophilicity of HfO_2:Hf film was enhanced by increasing pressure.

Fig. 7 shows the morphologies of HfO_2:Hf films deposited at pressures of (a) 1 Pa and (b) 3 Pa. The root-mean-square (RMS) roughness decreased with pressure. Because the probability of collisions of particles increased by increasing working pressure, it is probably why HfO_2:Hf film deposited at higher pressure had more adatom mobility and the relatively low surface roughness [28,29]. The roughness values were also very close to the morphologies of growing films [30]. In Fig. 7a and b, HfO_2:Hf films deposited at pressures of 1 Pa and 3 Pa exhibited a conic morphology and a tussocky morphology, respectively. The results indicated that the morphologies of HfO_2:Hf films were affected by working pressure significantly.

Fig. 8. shows the X-ray diffraction patterns of HfO_2:Hf films deposited at various pressures. The locations of diffraction peaks did not obviously change. It indicated that the structure of HfO_2:Hf films did not vary with pressure. Two broad diffraction peaks (110) and (111) were observed for the HfO_2:Hf film deposited at a pressure of 1 Pa. When the pressure

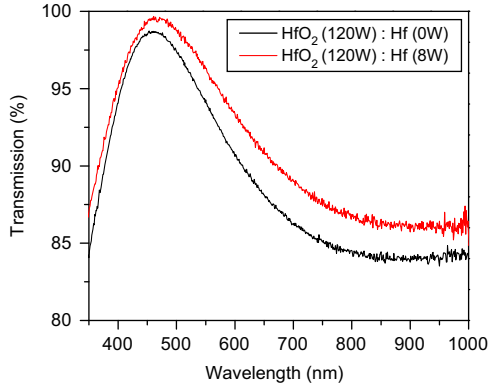

Fig. 5. The transmission in the UV–VIS–NIR region of HfO_2 and HfO_2:Hf films deposited at a pressure of 1.5 Pa.

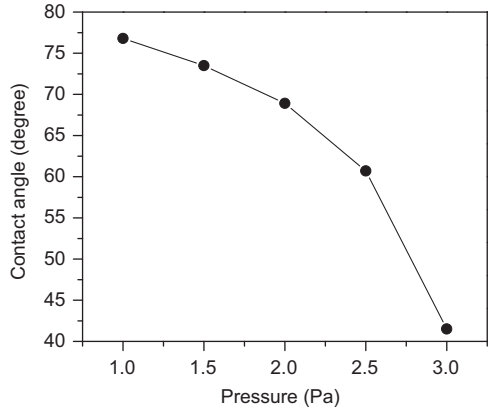

Fig. 6. Water contact angles on HfO_2:Hf films deposited at various pressures.

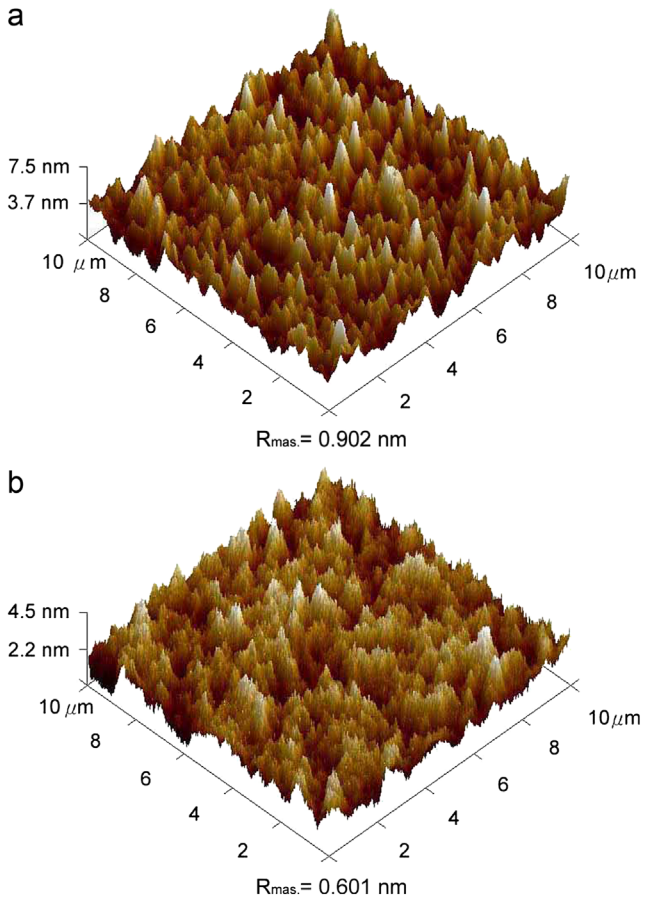

Fig. 7. The morphologies of HfO_2:Hf films deposited at pressures of (a) 1 Pa and (b) 3 Pa.

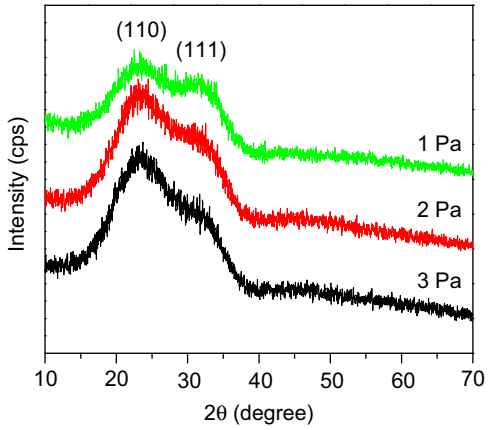

Fig. 8. The X-ray diffraction patterns of HfO_2:Hf films deposited at various pressures.

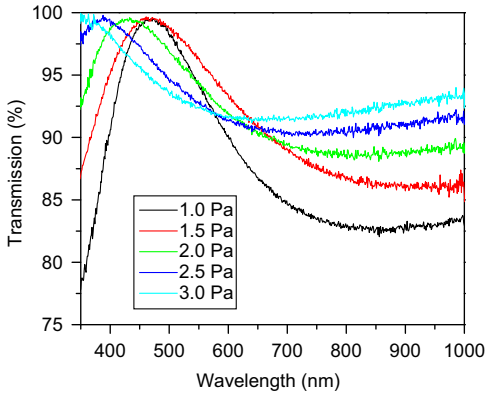

Fig. 9. The transmission in the UV–VIS–NIR region of HfO_2:Hf films deposited at various pressures.

increased, the intensity of the (110) peak increased, but the intensity of the (111) peak decreased.

According to the kinetics of crystal growth [31,32], the growing faces of a crystal are parts of the free surface of the film. These crystal faces corresponding to the final crystal shape are determined by the orientation of the crystal. A growth competition can start among the neighboring crystals in case of different orientations according to the types of their growing faces. The faster growing crystals will grow over the slower growing ones. This competition terminates when only crystals exhibiting the same type of crystal faces proceed to the free surface. This competitive crystal growth represents an orientation selection among the crystals, and results in the competitive growth texture [33]. This was probably why the nanocrystallinity of HfO_2:Hf film was closely related to pressure.

Fig. 9 shows the transmission in the UV–VIS–NIR region of HfO_2:Hf films deposited at various pressures. The optical transmission of HfO_2:Hf films strongly increased with pressure, especially in the ultraviolet region and near infrared region. It was probably due to the relatively low surface roughness, which could result in less light scattering [34].

Transparent materials generally exhibit the optical Kerr effect. Nonlinear refractive indices of materials are of great interest because of potential applications in designing optical devices and laser technology [35–38]. The refractive index, n, which depends on the radiation intensity, may be expressed in terms of the nonlinear refractive index n_2 ($cm^2\ W^{-1}$):

$$n\,(r,z) = n_o + n_2 I(r,z) = n_o + \Delta n(r,z) \tag{2}$$

where n_o is the linear refractive index, $I(r,z)$ is the irradiance of the laser beam within the sample, and $\Delta n(r,z)$ is the light-induced change in the refractive index. Based on the assumption that a Gaussian beam is traveling in the $+z$ direction, the beam irradiance can be written as

$$I(r,z) = I_0 \frac{\omega_0^2}{\omega^2(z)}\left[1-\frac{2r^2}{\omega^2(z)}\right] \tag{3}$$

where r is the radial radius of the imaginary sphere; $\omega_0$is the spot size of the beam at the focus; $\omega(z) = \omega_0\left(1+z^2/z_0^2\right)^{1/2}$ is the beam radius at a distance z from the position of the waist; $z_0 = \pi\omega_0^2/\lambda$ is the diffraction length of the Gaussian beam, and λ is the wavelength. The irradiance of the beam at the focus is denoted by I_0 and in terms of the input laser power, p_{in}, which equals to $2p_{in}/\pi\omega_0^2$. Therefore, for a Gaussian laser beam, the radial dependence of the irradiance gives rise to a radially-dependent parabolic refractive index change near the beam axis:

$$\Delta n(r,z) = n_2 I_0 \frac{\omega_0^2}{\omega^2(z)}\left[1-\frac{2r^2}{\omega^2(z)}\right] \tag{4}$$

Moiré deflectometry is a sensitive technique for measuring changes in the refractive indices of materials. The sensitivity of this technique is determined by the minimum measurable-angle of rotation (α_{min}). The tested sample was placed at various distances from the focal point of lens L_1, and the minimum angle of rotation was obtained. The same experiment was performed by using only a pure glass substrate to check the contribution of the glass substrate to the nonlinear refraction measurement. No observed fringe rotation or change in fringe size was found.

For the thin nonlinear medium of thickness d, the lowest nonlinear refractive index can be written as

$$n_{2,min} = \frac{\theta f_2^2}{2z_t}\frac{\pi}{2dp_{in}}\frac{\omega_0^4}{z_0^2}\alpha_{min} \tag{5}$$

and the change in the minimum refractive index is

$$\Delta n_{min} = \frac{\theta}{z_t}\frac{f_2^2\omega_0^2}{dz_0^2}\alpha_{min} \tag{6}$$

Fig. 10 shows the minimum nonlinear refractive indices and the change in the minimum refractive indices of HfO_2:Hf films deposited at various pressures on glass substrates. The nonlinear refractive index was measured to be of the order of $10^{-8}\ cm^2\ W^{-1}$ and the change in refractive index was of the order of 10^{-5}.

A change of the linear refractive index caused by stress is called the photoelastic effect [39]. The linear refractive index is specified by the indicatrix, which is an ellipsoid whose

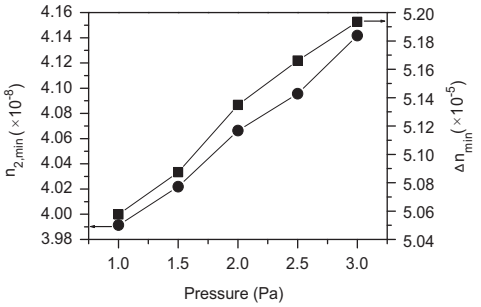

Fig. 10. The minimum nonlinear refractive indices and the change in the minimum refractive indices of HfO_2:Hf films deposited at various pressures on glass substrates.

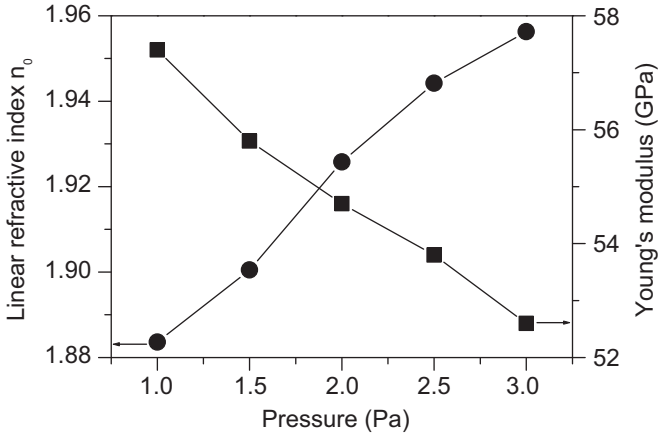

Fig. 11. The linear refractive indices and Young's moduli of HfO_2:Hf films deposited at various pressures.

coefficients are the components of the relative dielectric impermeability tensor B_{ij} at optical frequencies:

$$B_{ij}x_ix_j = 1 \tag{7}$$

The small change of the linear refractive index produced by stress is a small change in the shape, size and orientation of the indicatrix. This change is specified by the small changes in the coefficient B_{ij}.

If terms of higher-order than the first in the field of stresses are neglected, then the changes ΔB_{ij} in the coefficients are

$$\Delta B_{ij} = \varphi_{ijkl}\sigma_{kl} \text{ or } \Delta B_{ij} = p_{ijrs}\varepsilon_{rs} \tag{8}$$

where φ_{ijkl} and p_{ijrs} are called the piezo-optical and strain-optical coefficients, which typically have the orders of magnitude of 10^{-12} Pa^{-1} and 10^{-1} Pa^{-1}, respectively.

Based on the relation, $B = 1/n_0^2$, the change of linear refractive index for an isotropic film material is assumed to be [39,40]

$$\left(\frac{\partial n_0}{\partial \sigma}\right)_T = -\frac{1}{2}n_0^3\varphi \tag{9}$$

Consequently, a change in the linear refractive index due to film stress may affect the optical performance of an optical thin film, as shown in Eq. (9).

Fig. 11 shows the linear refractive indices and Young's moduli of HfO_2:Hf films deposited at various pressures. The linear refractive index of HfO_2:Hf film increased with pressure. However, the stress of HfO_2:Hf film decreased with pressure. The linear refractive index was found to correlate with the porosity [41,42]. It indicated that a dense HfO_2:Hf film with a high linear refractive index and low stress could be obtained by increasing pressure.

The value of $\Delta n_0/\Delta\sigma$ is reportedly similar to the stress-optical coefficient [43]. The stress-optical coefficient, $(\partial n_0/\partial\sigma)_T$, of a HfO_2:Hf film was evaluated to be in the range of -10.1×10^{-12} to -23×10^{-12} Pa^{-1}. Lower porosity corresponds to a lower stress-optical coefficient for the same material [42].

4. Conclusions

By doping with Hf, the lowest oxidation state of Hf (Hf^{0+}) presented preferentially and changed the hydrophobicity of HfO_2 film into hydrophilicity. On comparing with the HfO_2 film, the HfO_2:Hf film showed poor nanocrystallinity. For the HfO_2:Hf film, the structure did not vary with pressure, but the nanocrystallinity was closely related to pressure. The nonlinear refractive indices of HfO_2:Hf films deposited on the glass substrates were measured by Moiré deflectometry, and were of the order of 10^{-8} cm^2 W^{-1}. At higher pressure, the HfO_2:Hf film exhibiting a tussocky morphology corresponded to lower surface roughness and higher optical transmission. Better hydrophilicity, higher linear refractive index and lower stress-optical coefficient were obtained by increasing pressure.

Acknowledgments

The authors would like to thank the National Science Council of the Republic of China, Taiwan, for financially supporting this research under Contract no. NSC-100–2221-E-260-014.

References

[1] T. Nishide, S. Honda, M. Matsuura, M. Ide, Surface, structural and optical properties of sol–gel derived HfO_2 films, Thin Solid Films 371 (2000) 61–65.
[2] S.S. Lin, C.S. Liao, The hydrophobicity and optical properties of the HfO_2-deposited glass, Ceramics International 39 (2013) 353–358.
[3] Z.J. Wang, T. Kumagai, H. Kokawa, J. Tsuaur, M. Ichiki, R. Maeda, Crystalline phases, microstructures and electrical properties of hafnium oxide films deposited by sol–gel method, Journal of Crystal Growth 281 (2005) 452–457.
[4] A.R. Phani, M. Passacantando, S. Santucci, Synthesis and characterization of hafnium oxide and hafnium aluminate ultra-thin films by a sol–gel spin coating process for microelectronic applications, Journal of Non-Crystalline Solids 353 (2007) 663–669.
[5] Y. Wang, Z. Lin, X. Cheng, H. Xiao, Study of HfO_2 thin films prepared by electron beam evaporation, Applied Surface Science 228 (2004) 93–99.
[6] T. Mori, M. Fujiwara, R.R. Manory, I. Shimizu, T. Tanaka, S. Miyake, HfO_2 thin films prepared by ion beam assisted deposition, Surface and Coatings Technology 169–170 (2003) 528–531.
[7] Q. Fang, J.Y. Zhang, Z. Wang, M. Modreanu, B.J. O'Sullivan, P.K. Hurley, T.L. Leedham, D. Hywel, M.A. Audier, C. Jimenez,

J.P. Senateur, I.W. Boyd, Interface of ultrathin HfO_2 films deposited by UV-photo-CVD, Thin Solid Films 453–454 (2004) 203–207.
[8] X. Liu, D. Li, Influence of charged particle bombardment and sputtering parameters on the properties of HfO_2 films prepared by dc reactive magnetron sputtering, Applied Surface Science 253 (2006) 2143–2147.
[9] G. He, Q. Fang, G.H. Li, J.P. Zhang, L.D. Zhang, Structural and optical properties of nitrogen-incorporated HfO_2 gate dielectrics deposited by reactive sputtering, Applied Surface Science 253 (2007) 8483–8488.
[10] A. Deshpande, R. Inman, G. Jursich, C. Takoudis, Characterization of hafnium oxide grown on silicon by atomic layer deposition: interface structure, Microelectronic Engineering 83 (2006) 547–552.
[11] F. Meng, Z. Sun, Enhanced photocatalytic activity of silver nanoparticles modified TiO_2 thin films prepared by RF magnetron sputtering, Materials Chemistry and Physics 118 (2009) 349–353.
[12] W.T. Lim, C.H. Lee, Highly oriented ZnO thin films deposited on Ru/Si substrates, Thin Solid Films 353 (1999) 12–15.
[13] L. Gao, L. Zhou, J. Feng, L. Bai, C. Li, Z. Liu, J.L. Soubeyroux, Y. Lu, Stabilization of cubic structure in Mn-doped hafnia, Ceramics International 38 (2012) 2305–2311.
[14] T. Tan, Z. Liu, Y. Li, First-principles calculations of electronic and optical properties of Ti-doped monoclinic HfO_2, Journal of Alloys and Compounds 510 (2012) 78–82.
[15] M.K. Sharma, Aloke Kanjilal, Matthias Voelskow, D. Kanjilal, Ratnamala Chatterjee, Enhancement of ferromagnetism in Ni-implanted HfO_2 dielectric thin films, Nuclear Instruments and Methods B 268 (2010) 1631–1636.
[16] R. Lohmann, E. Österschulze, K. Thoma, H. Gärtner, W. Herr, B. Matthes, E. Broszeit, K.-H. Kloos, Analysis of r.f.-sputtered TiB_2 hard coatings by means of X-ray diffractometry and Auger electron spectroscopy, Materials Science and Engineering: A 139 (1991) 259–263.
[17] B.D. Cullity, Elements of X-ray Diffraction, Addison Wesley, Boston, MA, 1978, pp. 86–87.
[18] M. Oshima, S. Toyoda, T. Okumura, J. Okabayashi, H. Kumigashira, K. Ono, M. Niwa, K. Usuda, N. Hirashita, Chemistry and band offsets of HfO_2 thin films for gate insulators, Applied Physics Letters 83 (2003) 2172–2174.
[19] P.D. Kirsch, C.S. Kang, J. Lozano, J.C. Lee, J.G. Ekerdt, Electrical and spectroscopic comparison of HfO_2/Si interfaces on nitrided and un-nitrided Si(100), Journal of Applied Physics 91 (2002) 4353–4363.
[20] C.D. Wagner, W.M. Riggs, L.E. Davis, J.F. Moulder, G.E. Muilenberg, Handbook of X-ray Photoelectron Spectroscopy, Perkin-Elmer Corporation, Eden Prairie, MN USA, 1979.
[21] S. Suzer, S. Sayan, M.M.Banaszak Holl, E. Garfunkel, Z. Hussain, N.M. Hamdan, Soft X-ray photoemission studies of Hf oxidation, Journal of Vacuum Science and Technology A 21 (2003) 106–109.
[22] O. Renault, D. Samour, D. Rouchon, P. Holliger, A.M. Papon, D. Blin, S. Marthon, Interface properties of ultra-thin HfO_2 films grown by atomic layer deposition on SiO_2/Si, Thin Solid Films 428 (2003) 190–194.
[23] P.S. Bagus, F. Illas, G. Pacchioni, F. Parmigiani, Mechanisms responsible for chemical shifts of core-level binding energies and their relationship to chemical bonding, Journal of Electron Spectroscopy and Related Phenomena 100 (1999) 215–236.
[24] J. Yu, X. Zhao, Q. Zhao, Effect of surface structure on photocatalytic activity of TiO_2 thin films prepared by sol–gel method, Thin Solid Films 379 (2000) 7–14.
[25] D.V. Morgan, Y.H. Aliyu, R.W. Bunce, A. Salehi, Annealing effects on opto-electronic properties of sputtered and thermally evaporated indium-tin-oxide films, Thin Solid Films 312 (1998) 268–272.
[26] A.S. Guzenda, M.G. Lipman, H. Szymanowski, J. Kowalski, P. Wojciechowski, T. Halamus, A. Tracz, Characterization of thin TiO_2 films prepared by plasma enhanced chemical vapour deposition for optical and photocatalytic applications, Thin Solid Films 517 (2009) 5409–5414.
[27] I. Bernagozzi, S. Torrengo, L. Minati, M. Ferrari, A. Chiappini, C. Armellini, L. Toniutti, L. Lunelli, G. Speranza, Synthesis and characterization of PMMA-based superhydrophobic surfaces, Colloid and Polymer Science 290 (2012) 315–322.
[28] K. Koski, J. Hölsä, P. Juliet, Properties of aluminium oxide thin films deposited by reactive magnetron sputtering, Thin Solid Films 339 (1999) 240–248.
[29] D. Wang, U. Geyer, S. Schneider, G.V. Minnigerode, Grain sizes of Ni films measured by STM and X-ray methods, Thin Solid Films 292 (1997) 184–188.
[30] G. Laukaitis, S. Lindroos, S. Tamulevičius, M. Leskelä, Stress and morphological development of CdS and ZnS thin films during the SILAR growth on (100) GaAs, Applied Surface Science 185 (2001) 134–139.
[31] G. Knuyt, C. Quaeyhaegens, J. D'Haen, L.M. Stals, A quantitative model for the evolution from random orientation to a unique texture in PVD thin film growth, Thin Solid Films 258 (1995) 159–169.
[32] G. Knuyt, C. Quaeyhaegens, J. D'Haen, L.M. Stals, A model for thin film texture evolution driven by surface energy effects, Physica Status Solidi B 195 (1996) 179–193.
[33] P.B. Barna, M. Adamik, Fundamental structure forming phenomena of polycrystalline films and the structure zone models, Thin Solid Films 317 (1998) 27–33.
[34] T. Yamamoto, T. Shiosaki, A. Kawabata, Characterization of ZnO piezoelectric films prepared by rf planar-magnetron sputtering, Journal of Applied Physics 51 (6) (1980) 3113–3120.
[35] M.J. Soileau, W.E. Williams, N. Mansour, E.W. Van Stryland, Laser-induced damage and the role of self-focusing, Optical Engineering 28 (1989) 1133–1144.
[36] E.W. Van Stryland, Y.Y. Wu, D.J. Hagan, M.J. Soileau, K. Mansour, Optical limiting with semiconductors, Journal of the Optical Society of America B 5 (1988) 1980–1988.
[37] M.J. Soileau, W.E. Williams, E.W.Van Stryland, Optical power limiter with picosecond response time, IEEE Journal of Quantum Electronics QE-19 (1983) 731–735.
[38] K. Mansour, M.J. Soileau, E.W.Van Stryland, Nonlinear optical properties of carbon-black suspensions (ink), Journal of the Optical Society of America B 3 (1992) 1100–1109.
[39] J.F. Nye, Physical Properties of Crystals: Their Representation by Tensors and Matrices, Oxford Science, New York, 1992.
[40] W. Lukosz, P. Pliska, Determination of thickness, refractive indices, optical anisotropy of, and stresses in SiO_2 films on silicon wafers, Optics Communications 117 (1995) 1–7.
[41] G.S. Vicente, A. Morales, M.T. Gutierrez, Preparation and characterization of sol–gel TiO_2 antireflective coatings for silicon, Thin Solid Films 391 (2001) 133–137.
[42] S.S Lin, D.K. Wu, Enhanced optical properties of TiO_2 nanoceramic films by oxygen atmosphere, Journal of Nanoscience and Nanotechnology 10 (2010) 1099–1104.
[43] B. Hunsche, M. Vergöhl, H. Neuhäuser, F. Klose, B. Szyszka, T. Matthée, Effect of deposition parameters on optical and mechanical properties of MF- and DC-sputtered Nb_2O_5 films, Thin Solid Films 392 (2001) 184–190.